Hydraulic Control and Flow Separation in a Multi-Layered Fluid with Applications to the Vema Channel[1]

NELSON G. HOGG

Woods Hole Oceanographic Institution, Woods Hole, MA 02543

ABSTRACT

Observations from a recent field experiment in the Vema Channel are briefly described. These show a remarkable change in the configuration of isopycnal surfaces within the channel and the development of thick, nearly homogeneous regions near the bottom which are capped by sharp vertical gradients. Contrary to previous speculation that these "bottom boundary layers" result from enhanced vertical mixing, a dynamical mechanism is explored. This involves the hydraulic adjustment of an inertial, semi-geostrophic flow to the channel geometry.

First, an active two-layer flow in a rectangular geometry is studied to show that internal flow separation can occur when the flow is accelerated sufficiently by a narrowing channel. Almost always this separation accompanies hydraulic control: the slowest upstream moving Kelvin wave is stopped and upstream and downstream states are not symmetric with respect to the channel width. An active three-layer flow with a variable bottom profile is then presented as a more accurate model of the Vema Channel. The crucial geometrical ingredient appears to be the growth of a plateau on the eastern side of the channel: this confines the deepest layer laterally but it has more of a sill effect upon the upper layers. Many of the observed features of the flow are explained by this model including the changing layer shapes, flow separation, and the reverse flow found above the plateau.

A major disagreement is that the flow in the furthest downstream section does not appear to be separated, but more closely resembles that at the entrance. It is suggested that upstream of this last section a hydraulic jump occurs returning the flow to a subcritical state of lower energy. Consistent with this idea the potential energy of the deeper layers increases, and the wave perturbation amplitudes have the correct tendency.

1. Introduction

Relatively swift currents are found along the deep western boundaries of most ocean basins. These flows carry water away from polar sinking regions to temperate latitudes where it is gradually lost to the interior and returned poleward through vertical thermohaline circulation. This journey is interrupted by deep zonal ridges which separate the oceans into a number of smaller basins. In the South Atlantic the northward flow of Antarctic Bottom Water (AABW) is interrupted by several barriers including the Rio Grande Rise which divides the South Atlantic into the Argentine and Brazil Basins to the west of the Mid-Atlantic Ridge (Fig. 1.1a). Near the western boundary the top of the Rio Grande Rise (actually the Sao Paulo Plateau) is at ~3700 m depth, or approximately at the level of transition from north flowing AABW to south moving North Atlantic Deep Water (Reid *et al.*, 1977; Hogg *et al.*, 1982) and might, therefore, be considered a dam which determines this level in the Argentine Basin. However, the water does not spill over this dam uniformly. Instead it proceeds northward through a narrow, deep passage—the

Vema Channel—which cuts through the ridge and has a sill depth of ~4550 m some 850 m deeper than the ridge crest (see, Fig. 1.1b).

The flow of fluid through a constriction is a classical subject of fluid mechanics and engineering. In a more geophysical context, Whitehead *et al.* (1974) introduced the effect of rotation and showed that, when the flow is being controlled, the transport is related to upstream surface height through a modified wier formula. Observed flow rates and layer depths from three passages (Denmark Straits, Straits of Gibraltar and the Anegada Passage) were found to satisfy this formula reasonably well. The theory was elaborated by Gill (1977) who showed that the phenomenon of control was intimately associated with propagation of long wave disturbances: that is, control occurs when the fluid is accelerated to the point where long waves can no longer travel upstream at the control section (section of minimum width or depth or some function of the two). Gill (1977) also considered the upstream basin to be of finite depth as opposed to the infinitely deep basin of Whitehead *et al.* (1974).

Both these studies consider the channel geometry to be rectangular. In this situation as the flow accelerates under the constricting effect of the channel it
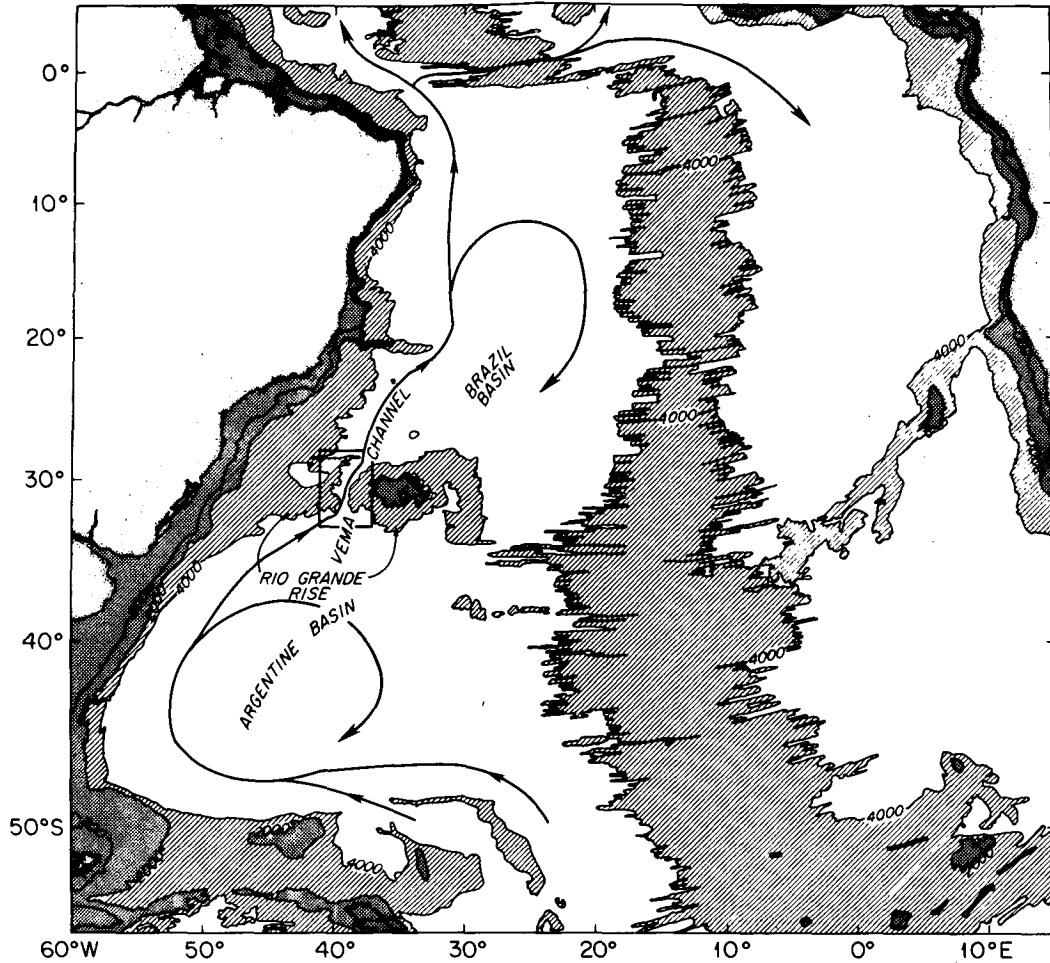
FIG. 1.1a. Bathymetry of the South Atlantic showing the Vema Channel as a break in the Rio Grande Rise. Arrows and streamlines indicate, schematically, the path of AABW. Adapted from Uchupi (1971).

becomes more and more banked against the right hand wall (looking downstream in the Northern Hemisphere). Near the control point (the narrowest section), either immediately upstream or downstream, the flow separates from the left wall and continues as a current along the right wall only. Clearly, if the only geometrical effect is a constriction of the sidewalls the separation point must occur downstream of the narrowest section.

This paper is concerned with the separation phenomenon and, in particular, with the possibility that in a multi-layered fluid, layers may separate internally, away from the bottom. The effects of stratification and rotation on the control problem have received little attention in the literature—the only related work of which this author is aware is the study of the Agulhas Current by Gill and Schumann (1979).

The principal motivation for this study comes from an attempt to explain the configuration of isopycnals observed in and near the Vema Channel during a recent field experiment (Hogg et al., 1982). In Fig.

1.2 are shown three representative vertical sections of potential density referenced to 4000 db (σ_4), one each from the inflow end (section 6), the middle (section 4) and the outflow (section 1). Section 4 is similar to all other sections made within the channel (8 in all) while sections 6 and 4 connect smoothly to other sections in the Argentine and Brazil Basins reported by Reid et al. (1977).

The intersection between North Atlantic Deep Water and AABW is near $\sigma_4 = 45.92$ (Reid et al., 1977; Hogg et al., 1982). Density surfaces with 45.87 $< \sigma_4 < 46.11$ slope downward from west to east geostrophically supporting a northward flow which intensifies downward in the expected sense. At the two extremities of the channel, sections 6 and 1 continue this tendency to the deepest shown isopycnal, $\sigma_4 = 46.13$. However, there is a reversal of this trend on section 4 such that isopycnals with $\sigma_4 > 46.11$ actually slope upward from west to east. A more detailed presentation is given in Fig. 1.3—potential temperature isotherms contoured from a "YO-YO" profiling sta-
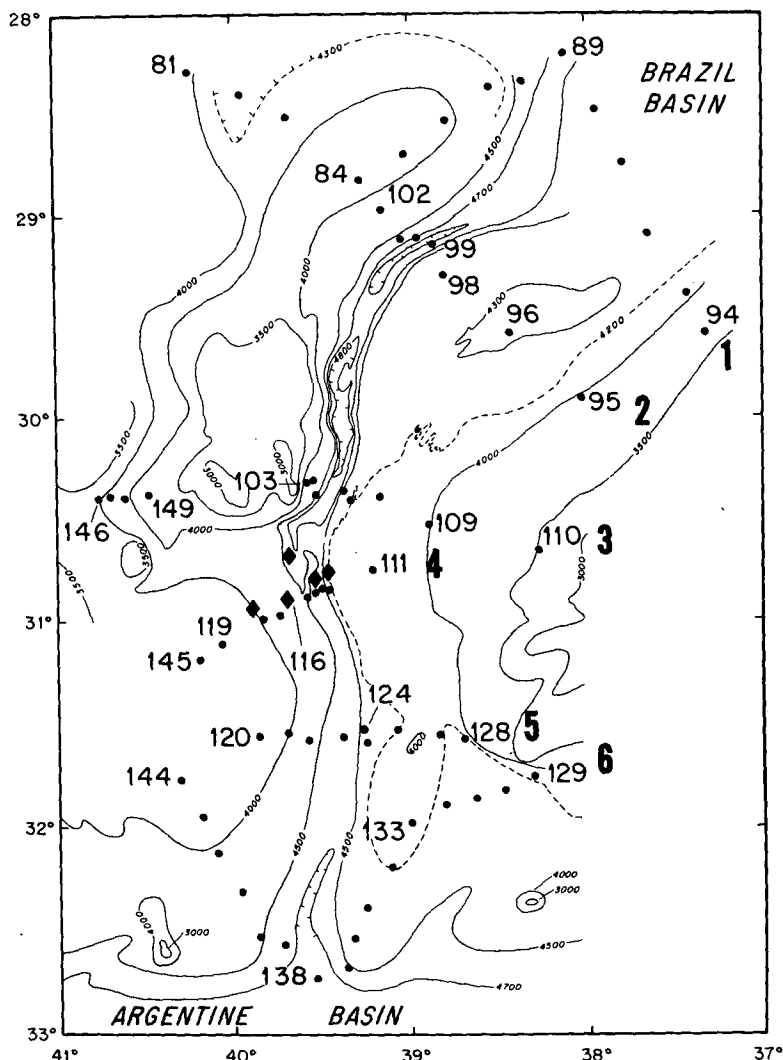
FIG. 1.1b. Bathymetry of the Vema Channel within the area indicated in Fig. 1.1a. Also shown are hydrographic stations (solid circles) from *Atlantis II*-107-leg 8 and mooring positions (solid diamonds). The region between the 4000 m isobath and the dashed 4200 m one on the east delineates a plateau south of 30°30'S which deepens to occupy the region between the 4200 and 4400 m isobaths further north. Large bold numbers to the right denote section numbers.

tion down the eastern wall of the channel on section 4 (essentially identical to a section reported by Johnson *et al.*, 1976). The reversal in isotherm slopes leads to a region of highly intensified vertical temperature gradient on the east wall which is further illustrated by the two temperature profiles in Fig. 1.4—the smooth one coming from the channel axis (station 115) while the stepped one is from the YO-YO portion (112 cast 1).

The bottom several hundred meters of both profiles in Fig. 1.4 are nearly homogeneous. Sarmiento *et al.* (1978) have taken this (and other similar property distributions, *e.g.*, dissolved radon gas) as evidence for large vertical mixing rates in the channel—rates that are at least two orders of magnitude greater than

those found elsewhere in the deep ocean. An alternative view, explored herein, is that these curious features result from a dynamical interaction between a broad western boundary current and the narrow Vema Channel through which it must flow. In this regard, note that the depth of the sharp vertical gradient in Figs. 1.3 and 1.4, ~4225 db, coincides with the depth at which the eastern wall of the channel (Fig. 1.2) levels off to form a broad plateau before rising again to the top of the Rio Grande Rise (see also Fig. 2 from Hogg *et al.*, 1982). This plateau will be considered to be the major geometrical characteristic of the channel: a constrictive effect which laterally confines the deepest water but vertically constrains the more shallow regions.
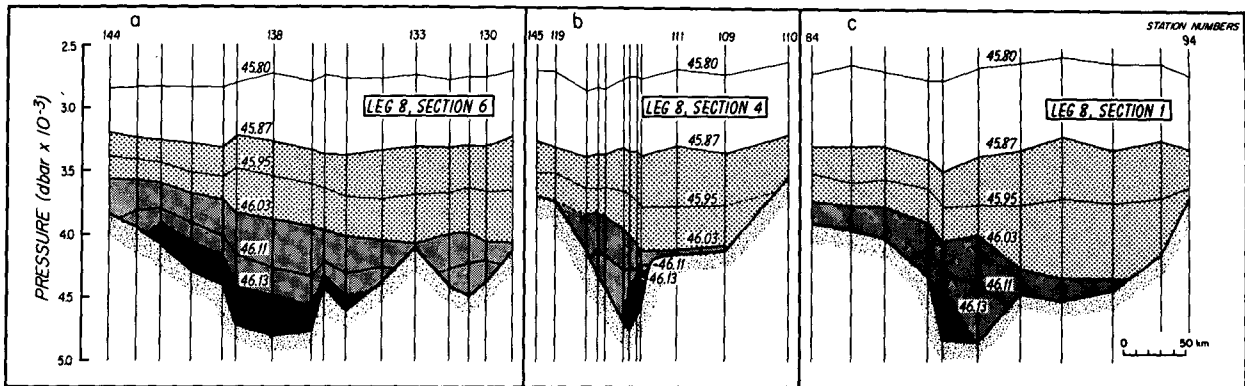
FIG. 1.2. Three cross sections of the channel showing depths of selected potential density surfaces σ_4; (a) section 6, (b) section 4 and (c) section 1. Section numbers refer to Fig. 1.1b.

Section 2 gives the mathematical formulation for the problem following Gill (1977) and Gill and Schumann (1979). In Section 3 the dynamical response of two moving layers to a rectangular channel is explored in which the only constriction comes from narrowing the channel. There are essentially three regimes in this situation—one of which results in the upper moving layer detaching from the left wall near the control point.

In Section 4 a three layer model with a variable bottom slope which more nearly resembles the Vema Channel is presented. Here the flow is dynamically constricted by the introduction of a plateau on the east side of an otherwise invariant channel geometry. The results of this model are discussed in Section 5

and related to the water properties described above. Conclusions are in Section 6.

2. Formulation

a. Semi-geostrophic equations

The following analysis closely follows that of Gill and Schumann (1979), and the reader is referred to that paper for a more rigorous justification of the assumptions and approximations. Their problem concerned the influence of varying longshore topography on a coastal jet; this work is an investigation of a broad, deep current confined by the walls of a channel. Consider the situation sketched in Fig. 2.1
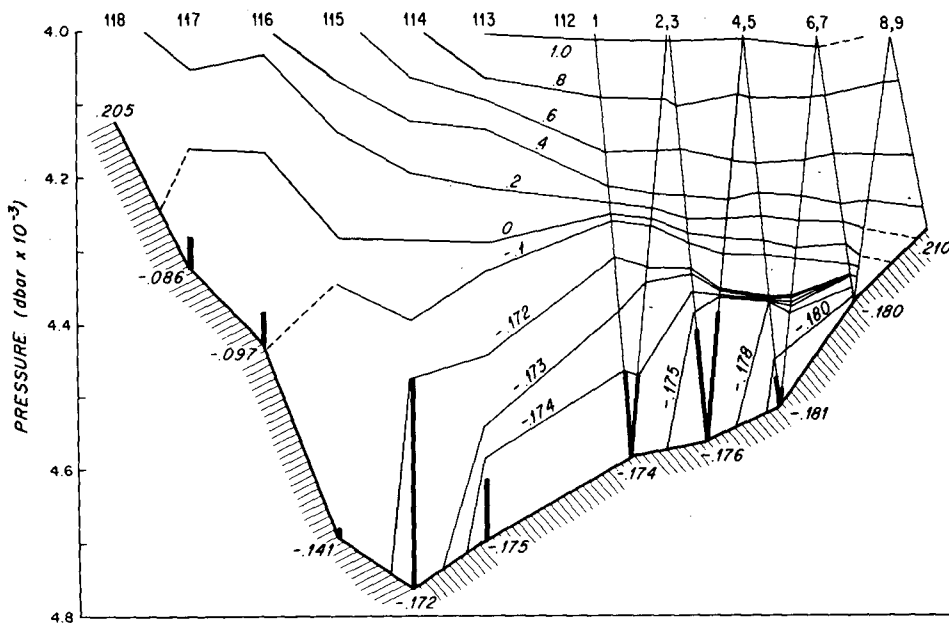
FIG. 1.3. Isotherms (potential temperature contours) for section 4 which include a YO-YO station up the eastern wall. Note the different horizontal scale for the YO-YO position and the variable temperature interval below 0°C. Thick vertical bars show regions in which temperature changes by less than 0.002°C.

in which homogeneous layers of fluid move along a channel of depth $H(x, y)$ under a resting layer which is deep enough that a reference level ($z = 0$) lies entirely within it. The z axis is vertical, the y axis along the local isobaths and the x axis perpendicular to it to form a right-handed cartesian system. If the channel is long with respect to its width and variations in the y direction are sufficiently slow, then the along-channel velocity component v will be much greater than the cross-channel component u. Provided that the time scale is no greater than the local inertial period and that dissipative effects are negligible, this narrow channel approximation results in the following semigeostrophic equations; geostrophic in the cross-channel balance but ageostrophic in the downstream balance:

$$fv_i = \frac{\partial(p_i/\rho_i)}{\partial x}, \tag{2.1}$$

$$\frac{\partial v_i}{\partial t} + \mathbf{u}_i \cdot \nabla_h v_i + f u_i = -\frac{\partial(p_i/\rho_i)}{\partial y}. \tag{2.2}$$

The subscript ($i = 1, N$) denotes layer number, p is pressure, ρ density and $\mathbf{u} = (u, v)$ the horizontal velocity vector. Each layer satisfies a shallow water continuity equation:

$$\frac{\partial D_i}{\partial t} + \nabla_h \cdot \bar{u}_i D_i = 0, \tag{2.3}$$
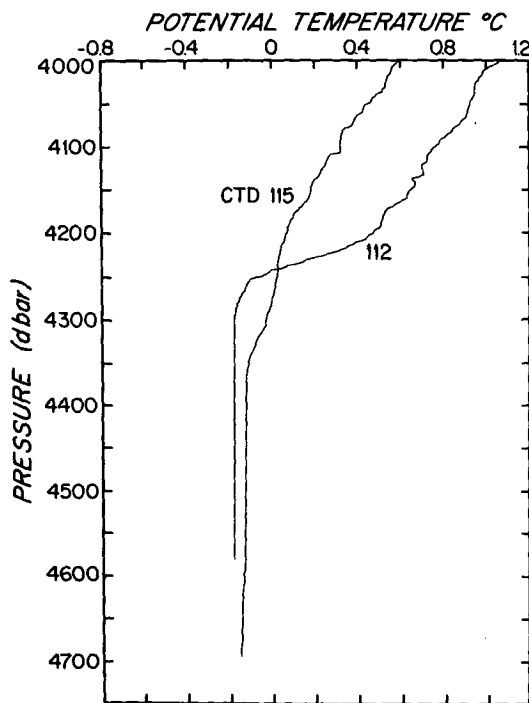
POTENTIAL TEMPERATURE °C

FIG. 1.4. Vertical profiles of temperature for stations 115 and the first case of station 112 (see Fig. 1.3) showing remarkably different vertical structure.
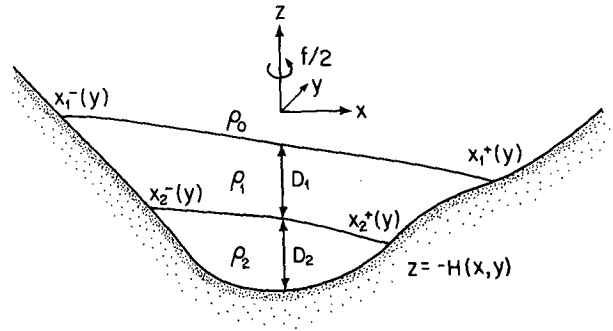

FIG. 2.1. Schematic diagram of model geometry.

and the vertical force balance is assumed hydrostatic so that the pressure in each layer can be related to its thickness (D_i) and density by

$$\frac{p_i}{\rho_i} = \frac{p_{i-1}}{\rho_{i-1}} - g_i\left(H - \sum_{j=i}^{N} D_j\right) \quad \frac{p_0}{\rho_0} = -gz, \tag{2.4}$$

with

$$g_i = g\left(\frac{\rho_i - \rho_{i-1}}{\rho_i}\right) \tag{2.5}$$

being the reduced gravity acting between layers.

Eqs. (2.1) and (2.2) can be combined into a vorticity equation by cross differentiation to eliminate pressure:

$$\left(\frac{\partial}{\partial t} + \mathbf{u}_i \cdot \nabla_h\right)\left[\left(f + \frac{\partial v_i}{\partial x}\right)D_i^{-1}\right] = 0. \tag{2.6}$$

For simplicity, the flow is assumed to have uniform potential vorticity within each layer and the latitude band of interest is assumed small enough that the planetary vorticity f can be treated as a constant. Therefore

$$\left[\left(f + \frac{\partial v_i}{\partial x}\right)D_i^{-1}\right] = \frac{f}{\hat{D}_i}, \tag{2.7}$$

where $\hat{D}_i$ is an upstream potential depth equal to the actual layer thickness at points where the relative vorticity vanishes. An equation for the Bernoulli potential B_i can be obtained from (2.2) rewritten in the form

$$\frac{\partial v_i}{\partial t} + \left(f + \frac{\partial v_i}{\partial x}\right)u_i = -\frac{\partial B_i}{\partial y}, \tag{2.8}$$

with

$$B_i = \frac{p_i}{\rho_i} + \frac{1}{2}v_i^2. \tag{2.9}$$

It is convenient to consider the above equations in nondimensional form. Taking $\hat{D}_1$ for a depth scale, $a = (g_1\hat{D}_1)^{1/2}f^{-1}$ (the Rossby radius of deformation) for the length scale, af for a velocity scale, f^{-1} for a time scale and $g_1\hat{D}_1$ for a pressure over density scale, the nondimensional equations become:

$$v_i = \frac{\partial p_i}{\partial x}, \tag{2.10}$$

$$\frac{\partial v_i}{\partial t} + \mathbf{u}_i \cdot \nabla_h v_i + u_i = -\frac{\partial p_i}{\partial y}, \tag{2.11}$$

$$\frac{\partial D_i}{\partial t} + \nabla_h \cdot \mathbf{u}_i D_i = 0, \tag{2.12}$$

$$p_i = p_{i-1} - \hat{g}_i[H - \sum_{j=i}^{N} D_j], \quad p_0 = 0. \tag{2.13}$$

with $\hat{g}_i = g_i/g_1$. The purely depth dependent term in the pressure, $-\rho_0 g z$, has been subtracted. Nondimensional vorticity and Bernoulli equations are

$$1 + \frac{\partial v_i}{\partial x} = \frac{D_i}{\hat{D}_i}, \tag{2.14}$$

$$\frac{\partial v_i}{\partial t} + \frac{D_i}{\hat{D}_i} u_i = -\frac{\partial B_i}{\partial y}, \tag{2.15}$$

$$\text{where} \quad B_i = p_i + \frac{1}{2}v_i^2. \tag{2.16}$$

Note that (2.10), (2.13) and (2.14) can be combined into a coupled set of inhomogeneous second-order differential equations in a single variable, $D_i - \hat{D}_i$:

$$\frac{\partial^2 p_i}{\partial x^2} = \frac{D_i - \hat{D}_i}{\hat{D}_i}$$

$$= \frac{\partial^2 p_{i-1}}{\partial x^2} - \hat{g}_i \left\{ \frac{\partial^2 H}{\partial x^2} - \sum_{j=i}^{N} \left[\frac{\partial^2}{\partial x^2} (D_j - \hat{D}_j) \right] \right\}. \tag{2.17}$$

The inhomogeneous term involves the second derivative of the bottom topography function, and for arbitrary $H(x, y)$ the equations must be integrated numerically subject to suitable boundary conditions. A further complication is that layer thicknesses will vanish somewhere on the sidewalls (positions $x = x_i^{\pm}$ on Fig. 2.1) or, under some circumstances, in the interior creating different dynamical regimes at whose boundaries matching conditions must be satisfied. In these situations the pressure and downchannel velocity component are matched across the boundary for each layer in order that the velocity and relative vorticity remain finite.

b. Steady flow

In the steady state (2.12) allows definition of a transport streamfunction:

$$\left. \begin{array}{c} u_i D_i = -\dfrac{\partial \psi_i}{\partial y} \\[2mm] v_i D_i = \dfrac{\partial \psi_i}{\partial x} \end{array} \right\}, \tag{2.18}$$

so that

$$\frac{\partial B_i}{\partial x} = \frac{\partial p_i}{\partial x} + v_i \frac{\partial v_i}{\partial x} = v_i \left(1 + \frac{\partial v_i}{\partial x} \right)$$

$$= D_i^{-1} \frac{\partial \psi_i}{\partial x}$$

using (2.16), (2.14) and (2.10). Therefore,

$$B_i = \psi_i D_i^{-1} + K_i, \tag{2.19}$$

where K_i is a constant of integration, yet to be determined [K_i has no y dependence from (2.15)]. If the total nondimensional transport in each layer is Q_i, the value of ψ_i at the left ($x = x_i^{-1}$) and right extremities ($x = x_i^{+}$) of each layer can be taken to be $\psi_i = -Q_i/2$ and $\psi_i = Q_i/2$, respectively. The Bernoulli constraint then gives boundary conditions for the coupled second-order differential equations of the form

$$p_i + \frac{1}{2}v_i^2 = \pm \frac{Q_i}{2\hat{D}_i} + K_i \quad \text{at} \quad x = x_i^{\pm}. \tag{2.20}$$

Far upstream, where the channel is presumed to open into a wide, flat bottomed basin the flow will be confined to currents along the boundaries with the relative strengths of left versus right being given by the value of the streamfunction in the interior $\hat{\psi}_i$. The constant K_i in (2.20) can then be specified using the hydrostatic equation (2.13) and the conditions that $v_i = 0$ and $D_i = \hat{D}_i$ in the interior. For a given distribution of layer thicknesses $\hat{D}_i$ and density ratios $\hat{g}_i$, the mean flow will be specified by the layer transports Q_i and the interior values of the streamfunction $\hat{\psi}_i$.

c. Wave motion

If the steady flow above is perturbed by small amplitude periodic disturbances of the form

$$v_i = v_i^*(x)\phi(y - ct), \quad u_i = u_i^*(x)\phi'(y - ct),$$

where ϕ is the arbitrary downchannel functional form, $u_i^*(x)$ and $v_i^*(x)$ give the cross-channel forms and c is the phase speed, the resulting motions will also satisfy the semi-geostrophic equations (2.10) to (2.13). Similar to Gill and Schumann (1979) it is possible to show that

$$p_i^* = p_{i-1}^* + \hat{g}_i \sum_{j=i}^{N} D_j^*, \tag{2.21}$$

$$\frac{\partial^2 p_i^*}{\partial x^2} = \frac{D_i^*}{\hat{D}_i}. \tag{2.22}$$

Boundary conditions are obtained from (2.15) with the stipulation that the cross-channel transport $D_i u_i$ vanish at the left and right boundaries of a layer. From the perturbed version of (2.15) it can be shown that

$$p_i^* + (v_i^\pm - c)\frac{dp_i^*}{dx} = 0 \quad \text{at} \quad x = x_i^\pm. \quad (2.23)$$

With uniform potential vorticity in each layer the only information needed about the steady flow is its strength at the layer boundaries $v_i^\pm$ and the potential depths $\hat{D}_i$. Where mean layer thicknesses vanish, either at the bottom or internally, the perturbation pressures p_i^*, and velocities v_i^* must be matched on either side.

Eqs. (2.21) and (2.22) with conditions (2.23) represent an eigenvalue problem for the phase speed c. There will be twice as many eigenvalues as there are layers, one set for internal Kelvin waves moving upstream and another for waves traveling downstream. In the one layer case, Gill (1977) has shown that hydraulic control occurs when the doppler shifted phase speed of the upstream traveling wave vanishes and that this coincides with an extremum in the channel geometry. In the multi-layer case where several internal modes are possible, the analysis will be restricted to the situation in which the upstream state is subcritical with respect to all modes and control occurs when the channel is narrow enough to stop the slowest moving mode.

Stopping just the slowest moving mode should only be considered to be "partial" control. It is also possible for a channel to completely control a stratified flow. In the nonrotating channel problem, Wood (1968) has shown that virtual control points can be found where the slower moving waves are stopped upstream of the real control (narrowest cross section). The layers essentially decouple and behave in a self similar manner, each resembling a one layer flow, and upstream layer thicknesses are uniquely determined by known volume transports and the channel geometry. The fluid layers in the Vema Channel highlighted in Fig. 1.2 do not behave in a self-similar manner and it must be concluded that, at best, only part of the baroclinic structure is being determined by this constriction.

3. Two-layer flow, rectangular channel

The simplest geometry in which to study rotating stratified hydraulics is the rectangular channel which has been used by both Whitehead et al. (1974) and Gill (1977). In the two layer case there are a number of parameters to specify: channel width and depth, density ratios, potential depths, layer transports and the division of this transport between upstream boundaries. In order to isolate the essentials of the stratified hydraulics problem (for Vema Channel applications, at least) only a small subset will be varied. The channel depth is fixed and control achieved through varying the width; layer depths and density ratios are taken equal ($\hat{D}_i = 1$, $\hat{g}_i = 1$), but the layer transport parameters Q_i and ψ_i are varied over a limited range.

In this way the upstream state is specified and the channel walls are narrowed to the minimum width (control width w_c) which is still consistent with the specified upstream state. This, invariably is found also to be the point at which the slowest upstream wave is stopped. In order not to change the upstream state, beyond this point in the channel the width must increase, and the solution smoothly switches to a different branch which is now supercritical. This procedure is somewhat backward from the usual physical situation in which the channel geometry is specified and the controlled upstream state then calculated.

With these simplifications (2.17) is a system of linear second-order homogeneous differential equations in $D_i - \hat{D}_i$ which are solved analytically. Four constants result and these are determined from the four boundary conditions (2.20). Special considerations must be given to situations in which an interface intersects the channel bottom or a layer thickness vanishes internally. The boundary conditions involve the square of the layer velocity and are, therefore, nonlinear. Solutions were found using the packaged subroutine ZSPOW from the International Mathematical Subroutine Library (IMSL). This approach also allowed introduction of further unknowns and constraints: for instance, the control width w_c could be found by permitting the channel width to be a variable and specifying that wave phase speed vanish; or the separation width w_s, at which a layer separates from the wall, could be determined by allowing width to vary and by specifying that a layer thickness vanish at the sidewall.

Given a specified upstream state (Q_i, $\hat{\psi}_i$, $\hat{D}_i$) the evolution of the layer thicknesses as the channel narrows to a control section and then widens once more was found to assume one of three characteristic states. For example, in Fig. 3.1 the layer depth configurations for three values of ψ_1 are shown ($Q_1 = Q_2 = 0.32$, $\psi_2 = 0$) as a function of the channel width. In Fig. 3.1a $\psi_1 = -0.5Q_1$ and all the transport for the upper moving layer is along the right boundary in the upstream basin and that for the lower layer is evenly split between both boundaries. The flow along the left boundary in the lower layer causes the interface to dip down and, as the channel narrows and the flow accelerates to conserve mass, this tilt increases. For widths more narrow than 0.68 nondimensional units no solutions are found which are continuous with those at slightly larger widths. At this point the slowest wave phase velocity vanishes: this is the control width—the minimum consistent with the chosen upstream conditions. As the channel is allowed to widen again, the solution switches in a smooth way to another branch and the lower interface continues to deepen on the left boundary: flow here is supercritical with respect to the slowest internal mode, and the lower layer accelerates much as water does after flowing over a dam. Eventually when the width becomes
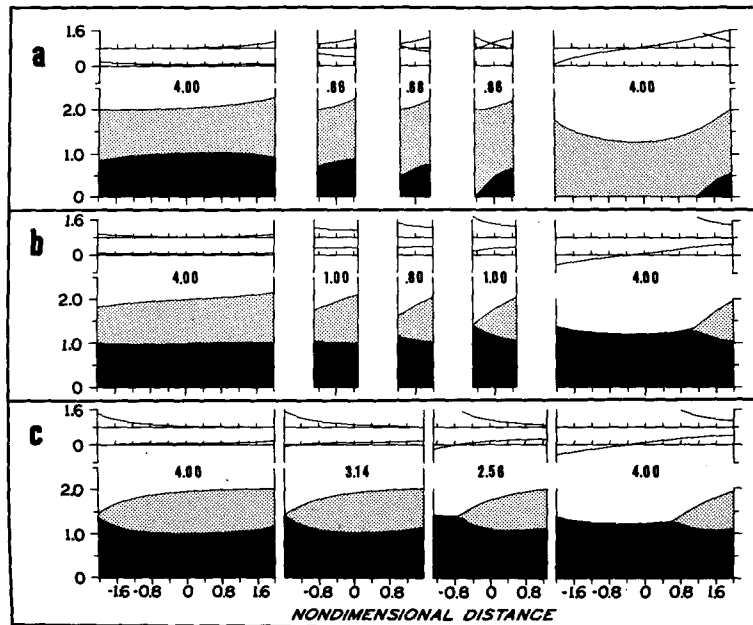
FIG. 3.1. Layer configurations (lower curves) and downchannel velocity (upper curves) for different values of $\hat{\psi}_1$ and different channel widths both upstream and downstream of the control section (narrowest). Number inserted into each configuration is the channel width. In each case the section at which flow separation occurs is also shown ($Q_1 = Q_2 = 0.32$, $\hat{\psi}_2 = 0.0$): (a) $\hat{\psi}_1/Q_1 = -0.5$; (b) $\hat{\psi}_1/Q_1 = 0.0$; (c) $\hat{\psi}_1/Q_1 = 0.5$.

greater than $w_s = 0.86$, the interface leaves the left wall, and the lower layer begins to hug the right one. These solutions, for the lower layer, look qualitatively similar to those given by Gill (1977) and Whitehead et al. (1974) for the one layer problem: loosely speaking the lower layer is hydraulically controlled.

When both layers have their upstream transport evenly distributed between boundaries ($\hat{\psi}_1 = \hat{\psi}_2 = 0$, Fig. 3.1b) the upper interface must now dip down at the left boundary while the lower one actually rises slightly upward yielding the same transport through lower speeds distributed over a thicker layer. Now as the channel narrows both these trends are increased: the upper layer on average gets thinner and the flow must accelerate more than in the lower layer which gets thicker. Control occurs for $w_c = 0.80$, and as the channel broadens downstream the upper layer steadily thins until it vanishes on the left wall for $w > w_s = 0.98$, beyond which point, the upper layer hugs the right hand wall. The one layer analysis might now be related to the upper layer.

Finally, if the upper layer transport in the upstream basin is confined to the left wall ($\hat{\psi}_1 = 0.5Q_1$, Fig. 3.1c) while the lower layer transport is evenly divided, as before; the lower interface tilts strongly upward against the left wall. A small change in width to $w_s = 3.14$ causes the upper layer to detach upstream of the control point which is achieved when the width becomes $w_c = 2.56$. The upper layer continues to

decrease in area in the supercritical region downstream.

The above discussion has been in terms of the simple concepts of mass continuity and geostrophy but it is a simple matter to see that these tendencies are consistent with potential vorticity and Bernoulli potential conservation. For instance in Fig. 3.1b when the upper layer shrinks along the left boundary its relative vorticity must decrease and the flow accelerates at the wall (see the downchannel velocity profiles at the top of each layer configuration plot). This acceleration decreases the pressure to conserve the Bernoulli potential and the lower layer rises. Its relative vorticity increases and the lower layer speed increases away from the boundary.

Which of the various states will be achieved in a given situation depends on the values of the various nondimensional parameters. In Fig. 3.2a the boundaries of the different regimes are shown in the $\hat{\psi}_1$-$\hat{\psi}_2$ plane for two cases in which the layer transports are equal. Here a fourth regime is identified in which the upper layer is everywhere separated from the left wall. Increasing the layer transports to $Q_1 = Q_2 = 0.89$ (dashed curves) greatly increases the extent of this region because interfacial tilts are magnified.

Having unequal transports in each layer causes the boundaries separating these regimes in $\hat{\psi}_1$-$\hat{\psi}_2$ space to move (see Fig. 3.2b). With larger transport in the upper layer (dashed curves) the region in which it is
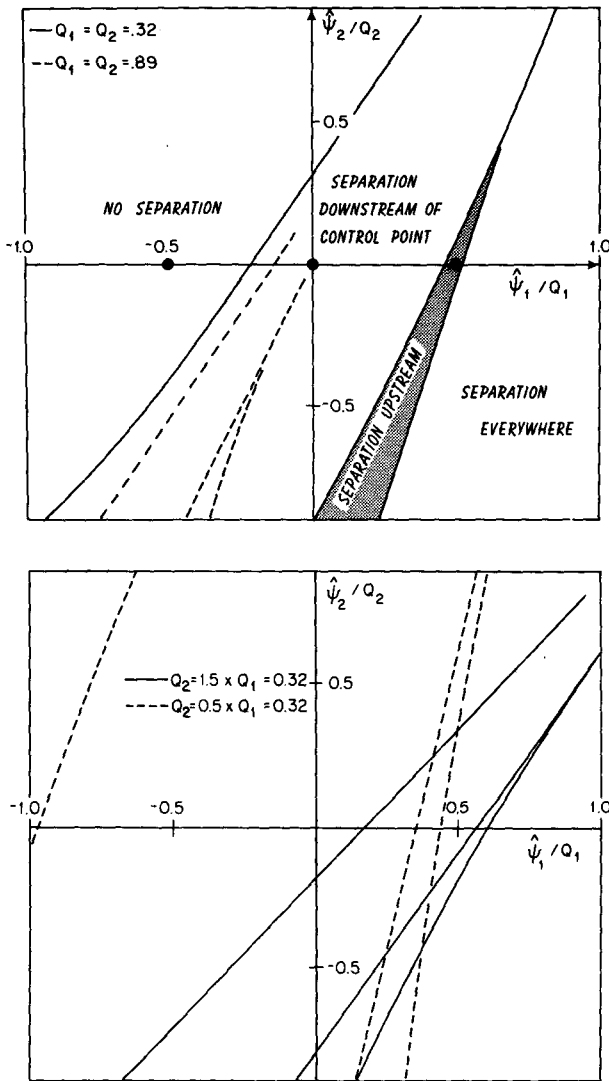
FIG. 3.2. The dependence of flow separation on $\hat{\psi}_1$ and $\hat{\psi}_2$ for (a) equal transport in each layer (solid dots show positions of solutions in Fig. 3.1) and (b) unequal transports in each layer. The shaded area is the only regime in which the upstream state is unseparated but separates before being controlled.

effectively controlled is larger. Likewise, decreasing the relative transport of the upper layer diminishes this region.

It is important to note that the region in which separation occurs upstream of the control width, but not everywhere (the shaded region in Fig. 3.2a), is quite small: with little qualification it can be said that the existence of a separated upper layer at some section when the upstream state is not separated is a strong indication that the flow is hydraulically controlled.

The channel widths (scaled by the Rossby deformation radius) at which control and layer separation are achieved, although generally order unity are a

strong function of the parameters involved. In Fig. 3.3 a plot is shown of w_s and w_c versus $\hat{\psi}_1$ ($\hat{\psi}_2 = 0$, $Q_1 = Q_2 = 0.32$). The control width varies from a minimum of ~0.6 at $\hat{\psi}_1 = -0.23Q_1$ to values well over 3.0 in the regime where the upper layer is always separated—the numerical scheme becomes inaccurate for nondimensional widths much greater than ~4. Except when the upper layer is either always or never separated the two widths are very nearly equal, another demonstration of the close dynamical link between the two phenomena.

4. Three-layer model, variable bottom

The two-layer rectangular channel model reveals the essential physics of the separation process and its links with hydraulic control. However, it is hardly a realistic model of flow through the Vema Channel. Referring back to the density sections of Fig. 1.2 and the discussion in Section 1 there appear to be three (somewhat arbitrary) density surfaces isolating layers which respond in characteristically different ways to the channel geometry. Water with $\sigma_4 < 45.87$ lies above the Rio Grande Rise and little change occurs as it flows north through the channel. Between $\sigma_4 = 45.87$ and $\sigma_4 = 46.03$ vertical columns thicken toward the east and this thickening increases on transit through the channel. The layer from $\sigma_4 = 46.03$ to $\sigma_4 = 46.13$ thickens on the west and thins on the east at mid-channel before relaxing back to a state similar to that seen upstream. Finally the layer with $\sigma_4 > 46.13$ is everywhere in contact with the bottom. It hugs the left wall at the entrance, swivels to hug the right wall in mid-channel and then rotates back on exit. There is a net loss in area of this layer—an indication that the flow may be hydraulically con-
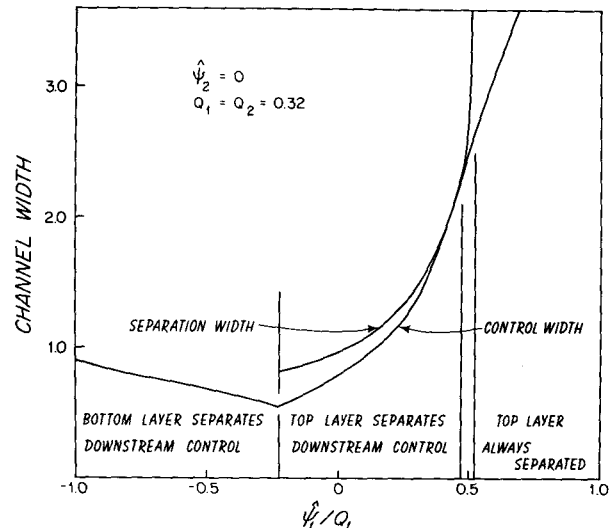

FIG. 3.3. Dependence of separation and control widths on $\hat{\psi}_1$ for $\hat{\psi}_2 = 0$, $Q_1 = Q_2 = 0.32$.

trolled for the flow is not symmetric between upstream and downstream states.

Using the formulation of Section 2, a three-layer model was developed which includes a variable bottom profile specified by the equation

$$H(x) = H\left[-1 + \tanh\left(\frac{x + \frac{1}{2}w}{s}\right) - \tanh\left(\frac{x - \frac{1}{2}w}{s}\right)\right]$$
$$- \frac{1}{2}H_p\left[1 - \tanh\left(\frac{x - x_p}{s_p}\right)\right]. \quad (4.1)$$

Unsubscribted parameters are appropriate to the channel and those subscripted by p are for an eastern plateau which is hypothesized to be the dynamically important constrictive effect. Only the plateau parameters are varied in the downstream direction. The constant H is the depth of the upstream basin away from the sloping boundaries where the width w becomes much larger than the width of the slope s. This depth is somewhat arbitrary and can be absorbed in the constant K_1 in (2.19). For example, in the upstream basin away from boundary layers,

$$\left.\begin{array}{l} p_1 = -\hat{g}_1[H - \sum_{j=1}^{3} \hat{D}_j] \\ v_1 = 0 \\ \psi_1 = \hat{\psi}_1 \end{array}\right\},$$

the constant K_1 can be set to zero and H determined by satisfying (2.19) subject to the above conditions.

The system of differential equations is now nonhomogeneous and possesses nonhomogeneous, nonlinear boundary conditions. They were solved iteratively in a two-step procedure. First, guessing at layer outcropping positions, the homogeneous form of the system of differential equations was integrated three times using three independent boundary conditions on the west wall which also satisfied the Bernoulli constraints there. The nonhomogeneous differential equation was then numerically integrated using homogeneous boundary conditions on the west wall to find a particular solution. The three homogeneous solutions could then be linearly combined with the nonhomogeneous solution and the amplitude factors determined by making the layer depths vanish on the east wall. Unless the initial outcrop positions were correct, the Bernoulli constraints on the east wall would not be satisfied. With these positions as unknowns, the IMSL routine ZSPOW was again used to iterate until these conditions were satisfied. Kelvinwave solutions were then determined using the velocities at the boundaries from the above calculation and numerically integrating the wave equations in Section 2c in a similar way such that the boundary condition (2.23) was satisfied on the west wall and the phase speed c varied until it was also satisfied on the east wall.

A large number of parameters is required to completely specify the flow. The geometrical parameters in (4.1) were taken to be

$$\left.\begin{array}{ll} w = 60 \text{ km}, & s = 15 \text{ km} \\ X_p = 5 \text{ km}, & s_p = 2 \text{ km} \end{array}\right\} \quad (4.2)$$

and the plateau height H_p was increased from zero until control was achieved and then decreased back to zero. The density difference across each interface was taken to be the same, 10^{-4} gm cm^{-3}. Upstream layer depths were chosen to be

$$\hat{D}_1 = 500 \text{ m}, \quad \hat{D}_2 = 450 \text{ m}, \quad \hat{D}_3 = 300 \text{ m}, \quad (4.3)$$

reflecting the tendency of layers to be thinner with depth on section 6, Fig. 1.2. Transports were taken to be (Sv):

$$Q_1 = 1.5, \quad Q_2 = 2.5, \quad Q_3 = 0.5, \quad (4.4)$$

in approximate agreement with Hogg et al. (1982). The most uncertain parameter is the division of this transport between upstream boundary layers as determined by $\hat{\psi}_i$. Rather arbitrarily, the values

$$\hat{\psi}_1/Q_1 = \hat{\psi}_2/Q_2 = 0.3, \quad \hat{\psi}_3/Q_3 = 0.7 \quad (4.5)$$

were chosen. For the upper two layers this implies that 80% of the transport is along the west wall and 20% along the east wall. For the lowest layer there is recirculation such that 0.1 Sv actually flows back along the eastern upstream boundary and 0.6 Sv flows in along the west.

None of the above values are particularly critical: the qualitative form of the result was found to be obtained over a range although it was not possible to explore the parameter space very exhaustively.

With the above specification of the problem isopycnal slopes and layer speeds were determined and are given in Fig. 4.1 for various heights of the eastern plateau. At the upstream end of the channel (H_p = 0 m) isopycnals slope uniformly down to the east except in regions on the left wall where layers vanish. Here the uniform potential vorticity constraint causes the relative vorticity to approach $-f$ as the layer vanishes and geostrophy gives the shown configuration. This is, perhaps, somewhat artificial but inspection of Fig. 1.2 shows that there is a similar tendency in the observed isopycnals. This change occurs over a Rossby radius—approximately 9 km in this example.

The true upstream state would be obtained in a much wider basin with a flat bottom and more gently sloping sides. Numerical inaccuracies prevented going beyond the 60 km width in single precision or 80 km in double. For the wider basin the flows do indeed continue to separate into boundary currents.

Raising the plateau 5 km to the east of the channel axis has the following dynamical effect on the mean state. The middle layer is squeezed on the east producing anticyclonic vorticity which accelerates the
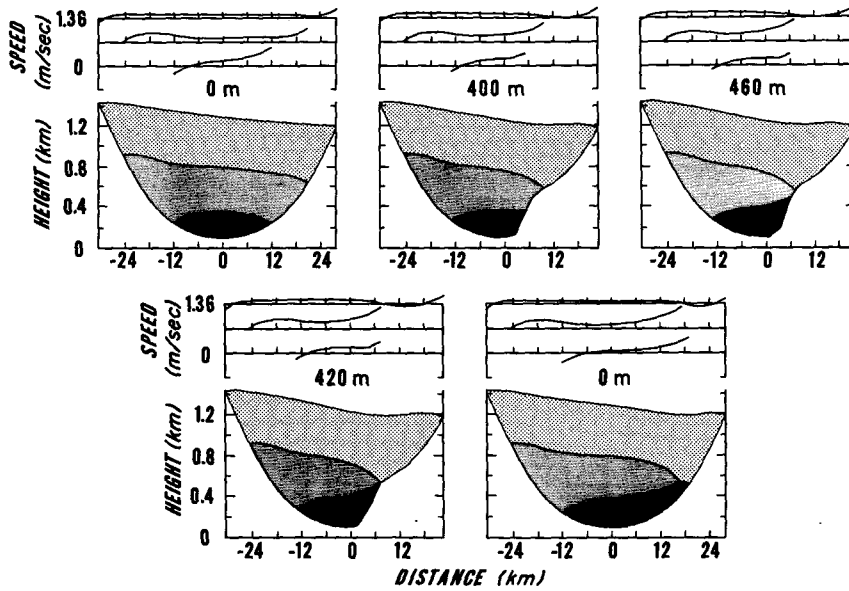
FIG. 4.1. A three layer model of flow through a channel with variable bottom relief. The only geometrical variable is the height of the plateau which rises 5 km east of the channel axis. The plateau height is given above each configuration.

flow closest to the eastern boundary (Southern Hemisphere). For the resulting increased shear to exist in geostrophic balance this layer's upper interface must tilt down, stretching the upper layer and inducing cyclonic vorticity which causes deceleration over the plateau: hence a developing region of weak southward flow. The acceleration of the middle layer also reduces the pressure felt by the lowest layer through the Bernoulli relation. Hence it rises but has little vorticity change because of the sloping bottom.

When the plateau height is ~460 m the slowest upstream moving Kelvin wave is stopped, and no solutions for higher plateaus match smoothly. This is the control point. As the height decreases again the solution proceeds continuously to a supercritical state, and at H_p = 420 m the lower interface has risen to the point that the middle layer begins to separate from the knee of the plateau (in the Southern Hemisphere). The separation depth coincides with the plateau height, and as the plateau is further lowered a finite region of separation exists at a depth very near the depth where separation first occurred.

5. Discussion and energetics

There are a number of similarities between the three layer model presented above and the actual flow conditions observed in the Vema Channel. The upper layer deepens toward the east, and the effect increases as the water goes through the channel. The consequent stretching of vortex columns induces a weak return flow over the plateau which increases toward the north. Of course, negative flow areas cannot con-

nect to the upstream state and, therefore, should be considered to come from different reservoirs of potential vorticity and Bernoulli potential. To account for this adequately seems an unnecessary complication at this point. The one current meter placed on the plateau shows weak southerly flow in the mean over a one-year record as contrasted with a strong $(7-21 \text{ cm s}^{-1})$ mean flow on instruments less than 10 km to the west over the channel axis (Schmitz and Hogg, 1982). All dynamically computed current sections from hydrographic data referenced to 3700 db show regions of weak southerly flow here, as well. This flow was also found to be essential in supplying water from the Brazil Basin to increase the salinity of the water coming from the south (Hogg et al., 1982). The non-mixing model of this paper gives a dynamical explanation for the existence of this weak flow.

When the middle layer detaches its thickness vanishes, and the relative vorticity must equal $-f$ for the potential vorticity to remain finite. In Fig. 5.1 cross stream velocity profiles are shown at 4250 db (the separation depth) computed with respect to 3700 dbar from the six hydrographic sections of Atlantis II-leg 8. The speed increases dramatically within the narrow confines of the channel, and the maximum shifts from the west to the east (compare with predicted profiles for the middle layer, Fig. 4.1). With this shift the cross stream gradient increases and for Section 4 (the best sampled) becomes very nearly equal to $-f$, consistent with the interpretation of the steep vertical gradients in Figs. 1.3 and 1.4 as being evidence of flow separation.
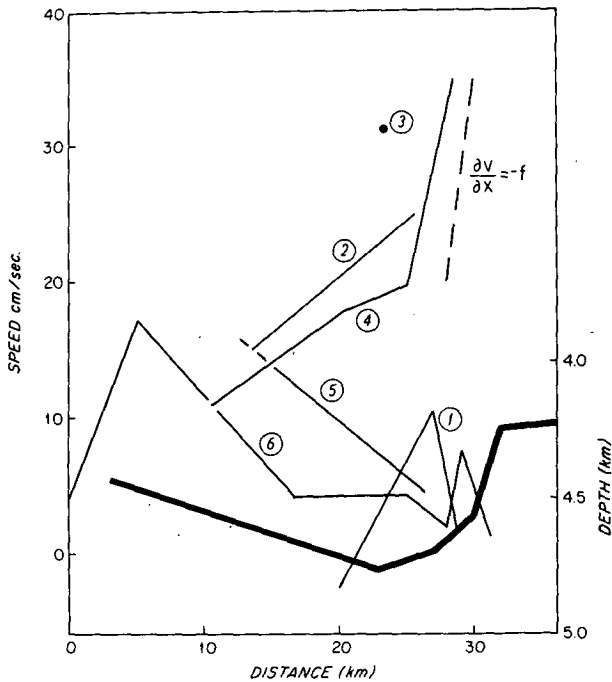
FIG. 5.1. Downchannel speed at 4250 dbar as a function of cross-channel distance calculated from hydrographic observations referenced to 3700 dbar for the six sections across Vema Channel. The heavy line shows the bottom depth on section 4 and the other sections have been plotted at their appropriate depths referenced to this section. Circled numbers refer to sections on Fig. 1.1b. (Note that on section 3 only one speed determination was possible.)

This intensified flow in the middle layer also causes the vertical velocity shear to reverse sign—a feature noted by Hogg et al. (1982) in a comparison of directly meandered currents and those computed geostrophically (their Fig. 8).

In Fig. 4.1 the flow separates at the knee of the plateau and the depth of the separated interface remains at this depth as the plateau subsides. This feature is also in approximate agreement with the observations (Fig. 1.2b and 1.3).

There is at least one aspect of the computed flow which is not in agreement with observations. In the Vema Channel, as the water pours out into the Brazil Basin (Fig. 1.2c), the isopycnals appear to relax back to a configuration similar to that observed at the upstream end (Fig. 1.2a) although, on average, they are somewhat deeper. The computed flow by comparison would have a separated flow continuing to accelerate as the walls widened into the downstream basin and becoming ever more supercritical with respect to the slowest Kelvin wave.

In more conventional nonrotating, one layer flows it is usual for the flow in this circumstance to undergo a hydraulic jump at some position downstream of the control section which is governed by conditions even farther downstream. This jump is stationary and allows the flow to become subcritical again by losing

energy but conserving mass and momentum. Potential energy increases across the jump but is more than offset by a larger loss of kinetic energy.

Assuming steady flow, it can be shown that the Bernoulli potential for a compressible adiabatic fluid can be written as (see Batchelor, 1967, p. 158)

$$B = \tfrac{1}{2}|\mathbf{u}|^2 + E + \alpha p + \phi, \qquad (5.1)$$

where $\alpha(T, S, p)$ is the specific volume (inverse of density) dependent on temperature T and salinity S as well as pressure. The internal energy (neglected in (2.16) is

$$E = -\oint p\,d\alpha, \qquad (5.2)$$

where integration is along a streamline and ϕ is the gravitational potential (geopotential)

$$\phi = gz = \phi_r - \int_{p_r}^p \alpha\,dp. \qquad (5.3)$$

Here ϕ_r is the potential of a reference surface assumed to be constant on $p = p_r$. The internal energy and pressure contributions can be integrated by parts:

$$E + \alpha p = \oint \alpha\,dp. \qquad (5.4)$$

It is usual to separate the specific volume into two parts, one of which removes most of the pressure dependence:

$$\alpha(T, S, p) = \alpha_0(0°C, 35‰, p) + \alpha'(T, S, p), \qquad (5.5)$$

with α' the specific volume anomaly.
The Bernoulli potential now becomes

$$B = \tfrac{1}{2}|\mathbf{u}|^2 + \phi_r + \oint^p \alpha_0(p)dp - \int_{p_r}^p \alpha_0(p)dp + \oint^p \alpha'dp - \int_{p_r}^p \alpha'dp. \qquad (5.6)$$

The pressure dependence of the combination of the first two integrals disappears so that if B_0 is the value of B at some reference position,

$$B - B_0 = \tfrac{1}{2}(|\mathbf{u}|^2 - |\mathbf{u}_0|^2) + \oint_{p_0}^p \alpha'dp - \int_{p_r}^p \alpha'dp. \qquad (5.7)$$

Tracing a streamline by the intersection of a potential density (σ_4) surface along the eastern boundary it is found that α' is very nearly constant, changing at most by a few percent. The last two integrals are related to the dynamic height anomaly D, so that

$$B - B_0 \triangleq \tfrac{1}{2}(|\mathbf{u}|^2 - |\mathbf{u}_0|^2) + \bar\alpha'(p - p_0) - 10(D - D_0) \qquad (5.8)$$

with $\bar\alpha'$ the average anomaly along the streamline.

In Fig. 5.2 the effective potential energy part of (5.8) is plotted for various isopycnals along the east

wall of the channel. Speeds required to make the total energy constant are also shown. For σ_4 = 46.05 and 46.10 the potential energy decreases monotonically from south to north. Comparing the speeds needed to make the kinetic energy compensate with those calculated in Fig. 5.1 it is plausible to think of the total energy being constant up to ~300 km after which it decreases, most markedly on the last section.

Below σ_4 = 46.10 the potential energy also decreases to about the 350 km point (Section 2), but a reversal occurs on the last section and the potential energy rises. Even though the isopycnals actually fall in section 6 (Fig. 1.2) this decrease in gravitational potential energy is more than offset by compressional increases in the internal energy and the effective potential energy rises. This is a highly depth dependent phenomenon, reflecting the baroclinic nature of the hydraulic effect, but is reminiscent of the nonrotating single-layer flow.

Pratt (1982) has numerically investigated the one layer rotating problem and shown that the hydraulic jump resembles a long Kelvin wave in which amplitude would decrease away from the eastern boundary in the Southern Hemisphere. Fig. 5.3 shows the cross-channel layer thickness distribution for the slowest moving Kelvin wave at the last section in Fig. 4.1. This mode is supercritical but, presumably, would propagate more quickly at finite amplitude and accommodate the transition to a subcritical state. The wave is high-mode baroclinic having its largest amplitude in the middle layer and opposing effects above and below. The amplitude tendencies are consistent with the observed changes, the middle layer thickens while those above and below get thinner and the up-

FIG. 5.3. Layer thickness perturbations for the small-amplitude supercritical Kelvin wave propagating in the furthest downstream mean state in Fig. 4.1. These are normalized such that the maximum value is unity.

per layer to the east of the separation point also thickens. Note that the thickness perturbation of the wave is not continuous across the separation point; however, the pressure is.

6. Conclusion

The steady, inertial flow of a multi-layered flow through a constriction can assume one of several different states in which different layers separate from the channel walls. A lateral constriction (rectangular channel) accelerates all layers of the flow and amplifies upstream interfacial slopes. The result is that if a layer is thinnest at the boundary it will become even thinner when the channel narrows. Given a specified upstream state, subcritical with respect to all wave modes, the channel can only narrow to a certain point (the control width) at which the slowest upstream wave becomes stationary. Downstream of this point the channel must widen, the flow becomes supercritical and the change in layer configurations continues to be amplified. If no layer has vanishing thickness in the upstream basin, one of the layers will pinch off and separate near the control point, almost always just downstream from it. Widths at separation and control are nearly equal.

These ideas have been applied to a model of the Vema Channel with more realistic bottom topography. The phenomenon of separation of an intermediate layer is offered as an explanation for the thick so-called bottom boundary layers observed in the
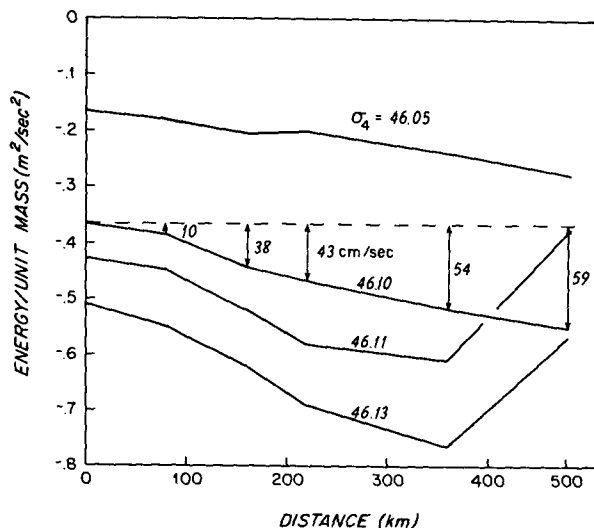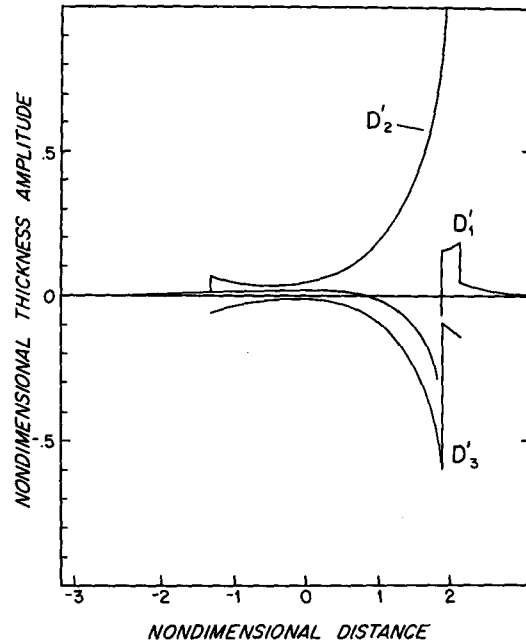

FIG. 5.2. Effective potential energy of various streamlines determined from where the indicated potential density surfaces intersect the east wall. Distance is measured from section 6. Speed values are those needed to make the total energy of the 46.10 surface uniform.

Vema Channel. It is suggested that these do not result from enhanced vertical mixing but instead are manifestations of the dynamic adjustment of the isopycnals to the narrow constriction.

This flow separation is circumstantial evidence that the flow is also hydraulically controlled—at least some part of the baroclinic structure is being determined by the channel in an analogous way to that in which a dam or a wier controls the level of water upstream of it. More direct evidence for hydraulic control is that the potential energy of deep streamlines falls along the eastern wall going through the channel but then rises abruptly upon entering the Brazil Basin—as though going through a hydraulic jump downstream of a dam. The supercritical baroclinic Kelvin wave has the form required to adjust the separated channel flow back to a non-separated, lower energy state which resembles that upstream.

There are some fundamental questions concerning stratified hydraulic control that have been glossed over in this analysis and remain unanswered. Most puzzling is the transition to continuous stratification where an infinity of vertical wave modes becomes possible with phase speed diminishing to zero as vertical mode number increases. Any upstream flow state would have to be initially supercritical with respect to these high mode numbers. What the implications are and what role friction might play are questions presently unanswered.

REFERENCES

Batchelor, G. K., 1967: *An Introduction to Fluid Dynamics.* Cambridge University Press, 615 pp.

Gill, A. E., 1977: The hydraulics of rotating-channel flow. *J. Fluid Mech.,* **80,** 641–671.

——, and E. H. Schumann, 1979: Topographically induced changes in the structure of an inertial coastal jet: Application to the Agulhas Current. *J. Phys. Oceanogr.,* **9,** 975–991.

Hogg, N. G., P. Biscaye, W. Gardner and W. J. Schmitz, Jr., 1982: On the transport and modification of Antarctic Bottom Water in the Vema Channel. *J. Mar. Res.,* **40** (Supp.), 231–263.

Johnson, D. A., S. F. McDowell, L. G. Sullivan and P. E. Biscaye, 1976: Abyssal hydrography, nephelometry, currents and benthic boundary layer structure in the Vema Channel. *J. Geophys. Res.,* **81,** 5771–5786.

Pratt, L. J., 1982: The dynamics of unsteady strait and sill flow. Ph.D. dissertation, MIT-WHOI Joint Program in Oceanography, 140 pp.

Reid, J. L., W. D. Nowlin, Jr., and W. C. Patzert, 1977: On the characteristics and circulation of the southwestern Atlantic Ocean. *J. Phys. Oceanogr.,* **7,** 62–91.

Sarmiento, J. L., W. S. Broecker and P. E. Biscaye, 1978: Excess bottom radon 222 distribution in deep ocean passages. *J. Geophys. Res.,* **83,** 5068–5076.

Schmitz, W. J., Jr., and N. G. Hogg, 1982: Exploratory observations of abyssal currents in the South Atlantic near Vema Channel. *J. Mar. Res.* (in press).

Uchupi, E., 1971: *The Bathymetric Atlas of the Atlantic, Caribbean, and Gulf of Mexico.* Tech. Rep. WHOI-71-71.

Whitehead, J. A., A. Leetmaa and R. A. Knox, 1974: Rotating hydraulics of strait and sill flows. *Geophys. Fluid Dyn.,* **6,** 101–125.

Wood, I. R., 1968: Selective withdrawal from a stably stratified fluid. *J. Fluid Mech.,* **32,** 209–223.